An improved method for seismic moment tensor inversion of acoustic emissions through assessment of sensor coupling and sensitivity to incidence angle

Title:

An improved method for seismic moment tensor inversion of acoustic emissions through assessment of sensors' coupling and sensitivity to incidence angle.

Authors:

Grzegorz Kwiatek (1), Elli-Maria Charalampidou (1), Georg Dresen (1), and Sergei Stanchits (2)

1. Helmholtz Centre Potsdam, GFZ German Research Centre for Geosciences, Telegrafenberg, D14473 Potsdam, Germany

2. TerraTek, a Schlumberger company, 1935 Fremont Drive, Salt Lake City, UT 84104, U.S.A.

Corresponding author:

Grzegorz Kwiatek, Helmholtz Centre Potsdam, GFZ German Research Centre for Geosciences, Telegrafenberg, D14473 Potsdam, Germany, email: kwiatek@gfz-potsdam.de, phone: +49 331 2881384

Abstract

Moment Tensor (MT) inversion is a standard tool allowing estimation of fault plane parameters as well as the amount of shear/volumetric change in the earthquake source. The inversion results depend on quality of P/S wave amplitude picks, sensor calibration and sensor coupling. However, the application of MT inversion to laboratory deformed rocks is difficult since coupling of the Acoustic Emission (AE) sensors is not easily assessed at experimental conditions in a pressure vessel. In this study, we present a procedure for the relative calibration of AE sensors and we analyze source processes of AE events recorded during two laboratory experiments on Bentheim and Vosges sandstones. We recorded AE activity and performed velocity measurements sending ultrasonic transmission (UT) pulses along different ray paths through the specimen. The first P-wave amplitudes of UTs were used to estimate the coupling quality of the AE sensors and sensor sensitivity as a function of incident angle for a specific frequency band. MT inversion was performed in both experiments using corrected and raw input amplitude data. We found that the quality of MTs improved significantly when data were corrected for coupling. We compared the developed procedure with the hybrid MT technique. Depending on sample and loading conditions, we observed significant compaction components in the MTs of AE events recorded in a test performed on Bentheim sandstone. The analysis of the Vosges sandstone sample was performed at low confining pressure producing AEs with mixed tensile-shear-compaction MT components.

Keywords:

Acoustic emissions; ultrasonic transmission; sensor calibration; moment tensor; focal mechanism; rock fracturing;

1 Introduction

AE analysis is frequently used in laboratory experiments as a method to describe the spatio-temporal evolution of damage. Furthermore, characterization of the AE sources provides insight into the micromechanical processes involved in the initiation and coalescence of cracks in rock samples [1]. AE source mechanism analysis provides additional information on the orientation and mechanisms of individual cracks during nucleation and formation of a fracture [2]. Simple techniques estimating the faulting mechanisms are based on average polarities [3] using dilatational and compressional first P-wave motions. This allows separating recorded AEs into tensile, shear and compaction sources. The moment tensor (MT) represents a measure of the deformation in the seismic source [4]. It is commonly used to provide information on fault plane parameters (strike, dip and rake of the fault). The decomposition of the MT allows estimating the ratio of the volumetric and non-volumetric strain in the seismic source [e.g. 5]. The MT inversion carries information on non-double couple (NDC) and double-couple (DC) components in earthquake sources, providing information on processes involved influid-induced seismicity [6, 7, 8, 9, 10] and mining-induced seismicity [11, 12, 13]. Collinset al. [14] investigated the source mechanisms of seismic events related to fracturingof tunnel walls. Sixteen AE sensors (frequency band 40-400kHz) were usedto calculate seismic MTs of extremely small seismic events (M_W<-5.0), most of which turned out to be DC seismic sources. Dahm [15] developed software for the relative seismic MT estimation and adapted it to one component piezoelectric sensors, typically used in AE measurements. The method was applied to studies performed in salt mines in Germany [16, 17, 18].

Manthei [19] determined the source mechanisms of AE events recorded during triaxial compression test on salt specimen. The calculated MTs indicated an NDCcomponent in good agreement with the recorded sample dilation. Most recently, Graham et al. [1] compared the polarity method [3] to the MT inversion usingfirst motion amplitudes [20, 21] of AE data recorded during triaxial compressionexperiments. Sellers et al. [2] used the hybrid MT inversion developed by Andersen [22] to calculate the MT of AE events recorded during a fracture experiment ona quartzite sample. Finally, Thompson et al. [23] investigated the focal mechanismof AEs and MTs of laboratory stick-slip experiments on Westerly granite tocorrelate source mechanisms with physical features observed on the fault plane.They suggested that the investigation of AE events provides a powerful analytical tool, which enables

a more complete qualitative understanding of rupture surface processes prior to dynamic instabilities in the laboratory.

The MT inversion procedure is sensitive to data quality and errors in polarities and picked amplitudes due to low signal-to-noise ratio conditions. Corrections for site effects and sensor characteristics strongly affect the results. MTs with spuriously high NDC components and/or strong biases introduced to the fault plane parameters may be observed. In addition, the MT inversion of events where the AE piezoelectric transducers were used is complicated because these sensors are not calibrated in an absolute sense in opposition to seismometers or accelerometers. Typically the amplitude response of AE sensors displays multiple resonant peaks. Moreover, the AE sensors are very sensitive to coupling to the specimen surface. Consequently, the MT results obtained from analysis of AE data are strongly affected by coupling and sensor characteristics. The MT tensors inversion results may be improved if sensors are calibrated using in-situ accelerometers located nearby [24]. However, AE sensor calibration is limited by the maximum frequency of the accelerometers.

To improve the quality of the seismic MT estimates of AE data recorded during laboratory tests on rock samples we developed a technique to assess the coupling quality of AE sensors and the sensitivity of the AE sensors as a function of the incidence angle. We test the procedure in two laboratory experiments performed on Bentheim and Vosges sandstone samples. The MT inversion results are compared to a hybrid moment tensor inversion technique suggested by Andersen [22].

2 Data

2.1 Experimental procedure

Dry cylindrical specimens from two quartz-rich porous sandstones (Vosges and Bentheim Sandstone) were first subjected to confining pressures of 50 and 160MPa, respectively. Subsequently, samples were loaded axially at constant displacement rate of 0.3µm/s (corresponding to a nominal axial strain rate of $4.2*10^{-6}s^{-1}$ and $3.3*10^{-6}s^{-1}$ for the Vosges and the Bentheim sandstone, respectively). AE and ultrasonic velocity measurements were recorded continuously during both experiments.

AEs were recorded by fourteen and sixteen P-wave AE sensors, glued directly to the surface of the Vosges and the Bentheim specimens, respectively. Sensors were sealed in a neoprene jacket with two-component epoxy and their location secured an appropriate azimuthal coverage of AE events (see Fig. 1, for the Bentheim specimen). These AE sensors consisted of PZT piezoceramic disks of 5mm diameter and 2mm thickness placed in brass housings, with a resonant frequency of 1MHz (with a typical recording frequency range between 0.3MHz and 0.8MHz). Additionally, two similar sensors (embedded in two metallic spacers) were placed at the top and bottom edges of the specimens. Detailed discussion on the

onset and evolution of the shear bands developed in the Vosges sandstone specimen have been characterized by means of acoustic and full-field methods [25]. Results on the initiation and propagation of the compaction bands, which developed in the Bentheim sandstone specimen, will be presented elsewhere.

All AE sensors were connected to a 16 channel transient recording system (DAXBox, PRÖKEL, Germany), with amplitude resolution of 16 bit at 10MHz sampling rate for the duration of the experiment. Signals were amplified by 40dB using Physical Acoustic Corporation preamplifiers. A series of P-wave velocity measurements was performed every 30 s, using ultrasonic transmission (UT) pulsesthat provided a time-dependent 1D velocity model composed of 5 horizontal and 1 vertical layers. During the UT measurements, a series of rectangular pulses of 100V amplitude was sent through the specimen using eight (for the Vosges sandstone) and nine (for the Bentheim sandstone) AE sensors (ultrasonic transmitters). These pulses were recorded on the remaining sensors (ultrasonic receivers) formingnearly 50 individual ultrasonic transmitter-receiver traces across each sample, during every UT measurement.

For each experiment, UT and AE waveforms were automatically discriminatedusing offline waveform processing software developed at GFZ [26]. The P-wave onsettimes of AE events and UT pulses were found by applying an automatic pickingalgorithm, based on the Akaike information criterion [e.g. 27], and followed by first P-waveamplitude measurements. The AE hypocenter locations were calculated byminimizing the travel time residuals using the simplex algorithm [28] taking intoaccount time-dependent 1D velocity model [26] estimated from UT measurements.The resolved location uncertainty of the AE events was about 2mm.

3 Method

3.1 Relative calibration

For seismic networks composed of seismometers or accelerometers, the sensor characteristics are known and the sensors are calibrated in an absolute sense (i.e. we know the amplitude response of the sensors in a certain frequency range). Commonly, potential site (or coupling) effects may be corrected. In contrast, AE sensors used in the laboratory experiments are not calibrated at elevated pressures and/or temperatures. The amplitude responses of AE sensors commonly display multiple resonant peaks and the coupling quality is not easily assessed at experimental conditions in a pressure vessel. In the following we propose the Ultrasonic Transmission Calibration (UTC) method that uses the UT data to assess the in-situ coupling quality of all AE sensors as well as the correction of recorded amplitudes for an incidence angle.

In a first step we ignore the frequency dependence of recorded signal amplitudes restricting the correction to signals with a dominant frequency band. The impulsive amplitude Ai recorded at ultrasonic receiver *i* generated by amplitude A_j produced by ultrasonic transmitter *j* is expressed as:

$$A_i = S_i I_i G_{ij} I_j S_j A_j \,, \tag{1}$$

where *S* is the sensor, *I* is the incidence angle and G_{ij} is the Green's function correction factors, respectively. Factors S_i and S_j incorporate site effects and transfer function of the ultrasonic receiver and transmitter at a certain frequency, respectively. We now assume that all sensors display the same behavior regarding dependence of the incidence angle on the recorded amplitudes. We model the incidence angle dependence using bell-shaped curve: $I_i = I_j = I(\alpha) = \exp\left(-a\alpha^b\right)$, where α is the angle of incidence to the ultrasonic receiver or equally the takeoff angle from the ultrasonic transmitter. This type of sensitivity of AE sensors to incident angles was previously found by Manthei [19]. The empirical coefficients *a* and *b* define the shape of the incidence angle correction curve. Since the amplitudes of the ultrasonic pulses are assumed to be the same for any transmitter, we assume A_j=1 and ignore this term in the correction procedure. Finally, we assume that the G_{ij} term contains only information on scattering: $G_{ij} \propto 1/R_{ij}$ (isotropic specimen), where R_{ij} is a distance between ultrasonic transmitter and receiver. The methodology is performing better for the experiments that do not display an extensive damage zones, especially if these zones are intersecting diagonally the whole sample (i.e. it may less reliable for stick-slip friction experiments on previously fractured samples where a broad damage zone is generated). Then equation 1 simplifies to:

$$A_{ij} = 1/R_{ij}\left[\exp\left(-a\alpha^b\right)\right]^2 S_i S_j \,, \tag{2}$$

where the unknowns are S_i, S_j , *a* and *b* using the information from amplitudes recorded at various sensors and their respective incidence angles. The inversion problem consists of fitting the amplitudes recorded during UT measurements, A_{ij}^{obs}, to those modeled with eq. 2. Estimated model coefficients are subsequently used to correct the recorded amplitudes of AE events for coupling and incidence angles. With progressive loading and increasing crack damage density the velocity field becomes increasingly anisotropic. The initial assumption of an isotropic medium used to estimate the Green's functions is then progressively rendered invalid.

3.2 Full Moment Tensor inversion

The full MT inversion was performed using software designed for mining-induced seismicity [29] based on the formal description presented in Fitch et al. [30] and Wiejacz [31]. The input data for the MT

inversion includes amplitudes of the first P-wave onset and the average rise time. The area below the first P wave pulse is assumed to be proportional to the seismic moment. Here we suggest a correction procedure providing a relative scaling of the estimated seismic moments.The MT inversion results in six independent MT components, which separate intoisotropic, compensated linear vector dipole and double-couple parts following the decomposition scheme of Knopoff and Randall [5]. The isotropic (=NDC) part ofthe MT describes changes in the volume of the AE source region. The remaining deviatoric part of the MT allows estimating the orientation of compressional and tensional axes, fault plane orientation and slip direction (strike, dip, and rake). The RMS error of the moment tensor inversion is calculated from the diagonal of the MT cross-correlation matrix. For both samples we uniformly selected the MT solutions with 14 P-wave picks, which is the maximum possible number of radialAE sensors that can be used.

3.3 Hybrid moment tensor inversion

We compared the developed UTC with the Hybrid Moment Tensor method (HMT), developed by Andersen [22]. This method aims at decreasing the influence of low quality observations, amplifying (or damping) signals that have been under- or overestimated by local effects at the sensor, and correcting for ray path focusing or defocusing due to inhomogeneities in the rock mass [2]. The HMT inversion is performed for a selected cluster of seismic events (located nearby), sharing similar travel paths from seismic sources to sensors to suppress the differences between Green's functions. Initially, the MT inversion is performed for each seismic event from an event cluster using the first P-wave ground displacement amplitudes. Afterwards, the resulting seismic moment tensors are used to predict the ground displacements at each sensor. The ratios $r_{ij} = r_{ij}^{\mathrm{th}} / r_{ij}^{\mathrm{obs}}$ are calculated for the synthetic and observed displacements for each station *i* and event *j*. Then, median values $\tilde{r}_i$ of ratios are estimated for each sensor separately, taking into account all events in the cluster. The median ratio for the specific station *i* is finally used to update the input displacement data according to the following scheme:

$$u_{ij}^{*,\mathrm{obs}} = u_{ij}^{\mathrm{obs}} + w_i u_{ij}^{\mathrm{obs}} \left(\tilde{r}_i - 1 \right), \tag{3}$$

where w_i is the arbitrarily chosen attenuation/weighting factor [22]. The seismic MTs are recalculated using the updated displacement data until $\left(\tilde{r}_i - 1 \right) < 0.01$, where $\left(\tilde{r}_i - 1 \right)$ is considered a site correction.

We calculated MTs of AE events using the HMT method. The input amplitude data from the MT inversion were updated according to equation 3 and the MTs of AE events were recalculated until the ratios r_{ij} converge towards a value close to 1 (i.e. no significant update to the input amplitudes).

4 Discussion

4.1 Relative calibration

With increasing load and increasing crack damage in the sample the amplitudes of the first P-wave UT pulses decrease (Fig. 2). The recorded AE amplitudes range from 20-600mV. Large differences in amplitudes between sensors at the beginning of the experiment result mainly from sensor coupling and different incidence angles. Average amplitudes for all possible ultrasonic transmitter-ultrasonic receiver pairs were selected from time window between 0 and 1000s corresponding to the initial part of the experiment (gray area in Fig. 2a).

Fig. 3a presents the relation between the relative UT amplitudes for Bentheim sandstone and the incidence angle of the ultrasonic transmission pulse at the UT receiver. Note that the recorded amplitudes generally decrease due to the increasing incidence angle, regardless of AE sensor. Furthermore, a few AE sensors clearly display lower amplitudes in comparison to other sensors for similar incidence angles. This observation is attributed to the quality of sensor coupling to the specimen. In particular, it is evident that sensors 10 and 13 display low quality coupling. Also, UT transmitter 8 (that forms a pair with ultrasonic receiver 6 shown in Fig. 3a) reveals low amplitudes at an incidence angle of 0°, indicating low quality coupling.

We compared the observed and modeled amplitudes using equation 2 and formed the following optimization problem: $\left\| A_{ij} - A_{ij}^{\mathrm{obs}} \right\|_{L1} = \min$, where *i* and *j* denote all possible ultrasonic transmitter-receiver pairs. The differences between observed and synthetic amplitudes were minimized using the simplex algorithm [28, 32]. Fig. 3b shows the resulting correction for Bentheim sandstone and thecorrection factors S_i. As expected, AE sensors 8, 10 and 13 require significant corrections (S_8 =3.24, S_{10} =3.37 and S_{13} =2.43) that are due to insufficient coupling of the sensors to the specimen. For the remaining sensors, the correction factors S_i, for this particular experiment, range between 1.00 and 1.16. We performed a similar correction for the experiment on Vosges sandstone (Fig. 4). Here, theinitial quality of coupling is good for all sensors, reducing the correction to theeffect of incidence angle.

4.2 Moment tensors

For the test performed on Bentheim sandstone, we selected 49591 events for theMT inversion. For the Vosges sandstone experiment, we calculated MTs for 1717 events. For both specimens, seismic MT inversions were performed using amplitudes calibrated using the UTC method and raw amplitudes, respectively (Fig.5). For AE events recorded during the Bentheim sandstone test, the correction routine significantly reduced the uncertainties of the MT inversion results. MTs calculated with and without corrections show only minor differences in uncertainties for the AE data from the test performed on Vosges sandstone. Here, all AE sensors show excellent coupling to the sample surface. As the ray coverage is almost the same in both experiments, we conclude that the large improvement ofthe quality of MTs

219 results from the correction of coupling problems of the sensors. The same applies to the case of Bentheim
220 sandstone when comparing MT solutions using amplitudes corrected for both coupling and incidence
221 angles with MT solutions calculated using amplitudes corrected only for coupling (not shown). This shows
222 that the effect of varying incidence angles on recorded AE amplitudes is small since the coverage with AE
223 sensors is very good and uniform in both experiments. Therefore, we observe comparable incidence angles
224 (normally around 40-50°) to most AE sensors. Consequently an incidence angle correction to these data is
225 not necessarily required for the MT inversion.
226 We compare the developed UTC with the HMT method using AE data from the Bentheim
227 sandstone test. As the number of AE events during the early part (0-1000s) of the experiment is small, we
228 extend the dataset and use also data from later stages (however, not exceeding T=4000s, cf. Fig. 2, for
229 which the P-wave amplitudes of UTs remains relatively stable). We select 6 spatio-temporal clusters
230 containing 116-212 AE events. Each cluster is composed of AE events that occurred within a distance not
231 exceeding 2mm from the center of the cluster and within a time window of 100s. The clusters were chosen
232 by scanning the whole sample for places that maximize the number of events in a sphere of certain radius
233 in a selected time window, however other clusters may be used as well provided that they contain enough
234 AE events. We impose these criteria to secure similar Green's functions for all events composing each
235 particular cluster. Although the criteria were chosen arbitrarily, we do not observe any significant changes
236 in the obtained results even when the size of the cluster is extended up to 4mm or we used broader time
237 window (up to 300s, both cases not shown here). The spatial distribution of the selected clusters is shown
238 in Fig. 6. We corrected the input data for the incidence angle to allow a comparison of UCT and HMT
239 method. We applied the HMT algorithm to each cluster separately assuming constant weighting factor
240 w_i=0.1 for all stations.
241 We performed the HMT inversion for a representative cluster A (Fig. 7). The amplitude ratios
242 converge to values close to unity after 30-40 iterations. Again, the largest corrections to the input
243 amplitude data are required for AE sensors 10, 13 and 8 (cf. Fig. 3) that have the lowest coupling quality.
244 Application of HMT method improves the quality of MT solutions for event cluster A (Fig. 7b) as well as for
245 the remaining clusters (not shown). Amplitude correction factors for each AE sensors are similar for HMT
246 and UTC methods but corrections are generally smaller when the HMT method is used.
247 Fig. 8 compares the amplitude correction factors obtained from the HMT method for all clusters
248 together with the coupling corrections assessed using UTC routine. The observed changes in amplitude
249 correction factors for each cluster may be attributed to its location and/or the time of the occurrence. We
250 found that the time of occurrence of each particular cluster does not affect significantly the estimated site

correction factors (not shown) in Bentheim sandstone. However, the correction factors are indeed sensitive to the location of the cluster due to the local differences in Green's functions. Unfortunately it is difficult to trace such changes since the effect of sample inhomogeneities on recorded amplitudes is unknown. The coupling correction factors from the here in proposed UTC and HMT method are in good agreement.

AE hypocenter locations in cross-section projections of the samples clearly show the compaction (Bentheim) and shear band (Vosges) formed during the test (Fig. 9a, b). The corresponding source type plots of [33] are shown as well. The shear band developed in the Vosges specimen and the compaction band developed in the Bentheim specimen are clearly imaged by clusters of AE hypocenters. The MT solutions of AE events shown in Fig. 9 were calculated using N=14 stations for both experiments. The black and gray points display decomposed MTs calculated with and without UTC calibration. Despite of larger scatter, the decomposed MTs calculated without UTC calibration frequently display inconsistent signs of isotropic and CLVD components (i.e. they fall in white quadrants of source type plots). This is likely a signature of lower quality of obtained MTs due to the use of uncalibrated data. The MT decomposition of UTC-calibrated AE events from the test performed on Bentheim sandstone displays mainly negative volumetric compaction-related and CLVD components. The NDC components may be related to collapse of pores and grain fracturing during compaction band formation and propagation [34, 25]. The formation of a shear band in the Vosges sandstone specimen produced AEs displaying a range of NDC and DC components of the MTs. Both positive (dilation) and negative (compaction) isotropic components are observed. We suggest that the NDC and DC components indicate cooperation of varying micromechanism during shearing such as cracking, grain shearing and compaction [e.g. 34, 25]. A more detailed analysis focusing on the temporal evolution of the recorded AE events is required for both sandstone specimens; however, this is beyond the scope of the present paper. It is also worth to note that the focal mechanisms of lower-quality AE data (relative RMS>0.05) from Vosges sandstone does not display compliant signs of isotropic and CLVD values (white areas of the source type plot in Fig. 9d). These events may be a signature of anisotropy in the sample due to the propagation of the shear band.

4.3 Conclusions

We present a new method providing an AE amplitude correction for site effects related to sensor coupling and incidence angle. The UTC procedure can be used in situations where the sensors are already located around a specimen that is placed inside the pressurized loading cell and one has to rely exclusively on waveforms recorded during the experiment in order to assess the coupling quality. We applied the method to calibrate the amplitudes of AE events generated in two different experiments, investigating

compaction band (Bentheim sandstone) and shear band formation (Vosges sandstone). We compared the RMS errors of moment tensors before and after application of the UTC and found that the method significantly reduces the uncertainties in MT results due to the combined effect of low coupling quality and incidence angle. We compared the UTC method with HMT inversion scheme. Both method yield similar correction factors for site/coupling effects, however the UTC procedure is not limited to small clusters of AE events as is the HMT method. In addition, our method allows correcting for the effect of incidence angle variation on recorded AE amplitudes. This is important for small number of piezoelectric sensors or unfavorable locations of sensors. The UTC method provides a global assessment of amplitude correction factors that is valid for the volume covered by travel paths of UT measurements.

References:

[1] Graham C, Stanchits S, Main I, Dresen G. Comparison of polarity and moment tensor inversion methods for source analysis of acoustic emission data, Int. J. Rock Mech. Min. Sci. 2010; 47: 161–169, doi: 10.1016/j.ijrmms.2009.05.002.

[2] Sellers E, Kataka M, Linzer L. Source parameters of acoustic emission events and scaling with mining-induced seismicity, J. Geophys. Res. 2003; 108: 2418, doi: 10.1029/2001JB000670.

[3] Zang A, Wagner FC, Stanchits S, Dresen G, Andresen R, Haidekker MA. Source analysis of acoustic emissions in Aue granite cores under symmetric and asymmetric compressive loads., Geophys. J. Int. 1998; 135: 1113–30.

[4] Gilbert F. Excitation of the normal modes of the earth by earthquake sources, Geophys. J. R. Astr. Soc. 1970; 22: 223–226.

[5] Knopoff L, Randall M. The compensated linear-vector dipole. A possible mechanism for deep earthquakes, J. Geophys. Res. 1970; 75: 1957–1963.

[6] Ross A, Foulger G, Julian B. Non-double-couple earthquake mechanisms at the Geysers Geothermal Area, California, Geophys. Res. Lett. 1996; 23: 877–880, doi: 10.1029/96GL00590.

[7] Vávryčuk V, Bohnhoff M, Jechumtálová Z, Kolár P, Šílený J. Non-double-couple mechanisms of microearthquakes induced during the 2000 injection experiment at the KTB site, Germany: A result of tensile faulting or anisotropy of a rock?, Tectonophysics 2008; 456: 74–93, doi: 10.1016/j.tecto.2007.08.019.

[8] Fischer T, Guest A. Shear and tensile earthquakes caused by fluid injection, Geophys. Res. Lett. 2011; 38: L05307, doi: 10.1029/2010GL045447.

[9] Benson PM, Vinciguerra S, Meredith PG, Young RP. Laboratory Simulation of Volcano Seismicity. Science 2008; 322: 249–252.

[10] Benson PM, Vinciguerra, S, Meredith, PG, Young, RP. Spatio-temporal evolution of volcano seismicity: A laboratory study. Earth Planet. Sci. Lett. 2010; 297: 315–323.

[11] Wiejacz P. Calculation of seismic moment tensor for mine tremors from the Legnica-Głogów Copper Basin, Acta Geophys. Pol. 1992; 40: 103–122.

[12] Šílený J, Milev A. Seismic Moment Tensor Resolution on a Local Scale: Simulated Rockburst and Mine-induced Seismic Events in the Kopanang Gold Mine, South Africa, Pure Appl. Geophys. 2006; 163: 1495–1513, doi: 10.1007/s00024-006-0089-z.

[13] Gibowicz SJ, Harjes H-P, Schäfer M. Source parameters of seismic events at Heinrich Robert mine, Ruhr Basin, Federal Republic of Germany: Evidence for non-double-couple events, Bull. Seismol. Soc. Am. 1990; 80: 88–109.

[14] Collins D, Pettitt W, Young R. High-resolution Mechanics of a Microearthquake Sequence, Pure Appl. Geophys. 2002; 159: 197–219, doi: 10.1007/PL00001251.

[15] Dahm T. Relative moment tensor inversion based on ray theory: Theory and synthetic tests, J. Geophys. Res. 1996; 124: 145–257.

[16] Dahm T, Manthei G, Eisenblätter J. Relative moment tensors of thermally induced microcracks in salt rock, Tectonophysics 1998; 289: 61–74.

[17] Dahm T, Manthei G, Eisenblätter J. Automated moment tensor inversion to estimate source mechanisms of hydraulically induced micro-seismicity in salt rock, Tectonophysics 1999; 306: 1–17.

[18] Manthei G, Eisenblätter J, Spies T. Source parameters of acoustic emission events in salt rock, J. Acoustic Emission 2001; 19: 100–108.

[19] Manthei G. Characterization of acoustic emission sources in a rock salt specimen under triaxial compression, Bull. Seismol. Soc. Am. 2005; 95: 1674–1700.

[20] Ohtsu M. Simplified Moment Tensor Analysis and Unified Decomposition of Acoustic Emission Source: Application to in Situ Hydrofracturing Test, J. Geophys. Res. 1991; 96: 6211–6221, doi: 10.1029/90JB02689.

[21] Ohtsu M. Moment tensor analysis of AE and SiGMA code, In: Kishi T, Ohtsu M, Yuyama S (Eds.), Acoustic Emission—Beyond the Millennium, Elsevier, Amsterdam; 2000, p. 19–34.

[22] Andersen L. A relative moment tensor inversion technique applied to seismicity induced by mining, PhD. thesis, Univ. of the Witwatersrand, Johannesburg; 2001.

[23] Thompson B, Young R, Lockner D. Premonitory acoustic emissions and stick-slip in natural and smooth-faulted Westerly granite, J. Geophys. Res. 2009; 114: B02205, doi: 10.1029/2008JB005753.

[24] Kwiatek G, Plenkers K, Dresen G. Source Parameters of Picoseismicity Recorded at Mponeng Deep Gold Mine, South Africa: Implications for Scaling Relations, Bull. Seismol. Soc. Am. 2011; 101: 2592–2608, doi: 10.1785/0120110094.

[25] Charalampidou E-M, Hall S, Stanchits S, Lewis H, Viggiani G, Characterization of shear and compaction bands in a porous sandstone deformed under triaxial compression, Tectonophysics 2011; 503: 8–11.

[26] Stanchits S, Vinciguerra S, Dresen G. Ultrasonic Velocities, Acoustic Emission Characteristics and Crack Damage of Basalt and Granite, Pure Appl. Geophys. 2006; 163: 975–994, doi: 10.1007/s00024-006-0059-5.

[27] Leonard M, Kennett B. Multi-component autoregressive techniques for analysisof the seismograms, Phys. Earth Planet. Int. 1999; 113: 247–263, doi: 10.1016/S0031-9201(99)00054-0.

[28] Nelder J, Mead RA. Simplex method for function minimization, Comput. J. 1965; 7: 308–313.

[29] Kwiatek G. FOCI — Software for calculation of the seismic momenttensor and source parameters in mining environment, URL: http://www.sejsmologia-gornicza.pl/projekty/foci, 2011.

[30] Fitch TJ, McCowan DW, Shields MW. Estimation of seismic moment tensor from teleseismic body wave data with application to intraplate and mantle earthquakes, J. Geophys. Res. 1980; 85: 3817–3828.

[31] Wiejacz P. Badanie mechanizmów wstrząsów górniczych przy wykorzystaniutensora momentu sejsmicznego, PhD thesis, Institute of Geophysics, Polish Academy of Sciences, Warszawa, 1992.

[32] Lagarias J, Reeds J, Wright M, Wright P. Convergence Properties of theNelder-Mead Simplex Method in Low Dimensions, SIAM J. Optimization. 1998; 9: 112–147, doi: 10.1137/S1052623496303470.

[33] Hudson J, Pearce R, Rogers RM. Source type plot for inversion of the momenttensor, J. Geophys. Res. 1989; 94: 765–774.

[34] Stanchits S, Fortin J, Gueguen Y, Dresen G. Initiation and propagation ofcompaction bands in dry and wet Bentheim sandstone, Pure Appl. Geophys. 2009; 166: 843–868, doi:10.1007/s00024-009-0478-1.

Figure captions

Fig. 1: Schematic view of the network setup for the Bentheim sandstone specimen. The locations of AE sensors glued to the sample surface are marked using points and numbers with color reflecting the operation mode during ultrasonic transmission measurements (red for ultrasonic transmitters and blue for ultrasonic receivers, respectively). Examples of idealized ultrasonic P-wave pulse ray paths sent by various ultrasonic transmitters and recorded by receiver 7 are shown using dashed gray lines.

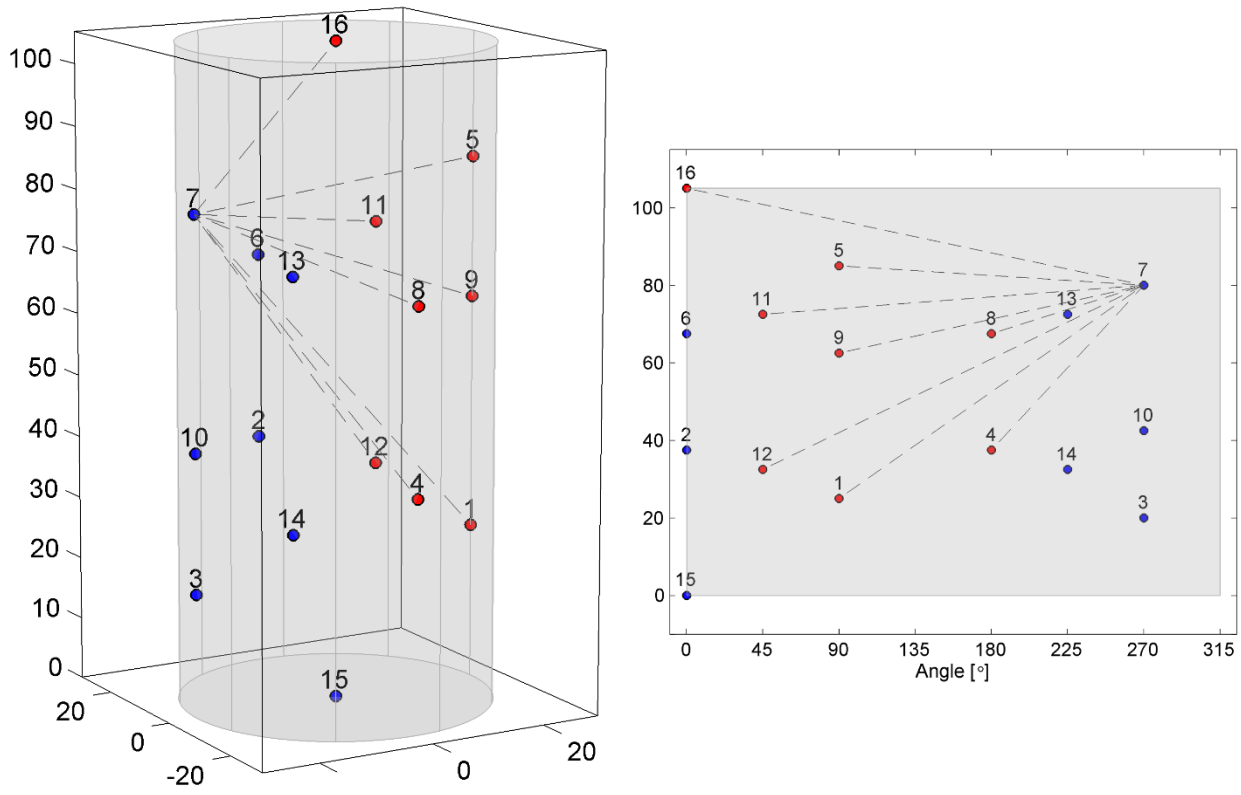

Fig. 2: (a): Changes in recorded amplitudes of first P-wave UT pulses from the Bentheim specimen sent by various ultrasonic transmitters and recorded at ultrasonic receiver 7 (cf. Fig. 1) as a function of time. The amplitudes are corrected for distance only. The amplitudes are decreasing with time due to the increasing damage. The symbols mark the average value of amplitude calculated for the time period 0-1000 s (shaded area) for each ultrasonic transmitter-receiver pair that was used for the relative calibration. (b): Changes in the average value of amplitude calculated versus the equivalent incidence angle.

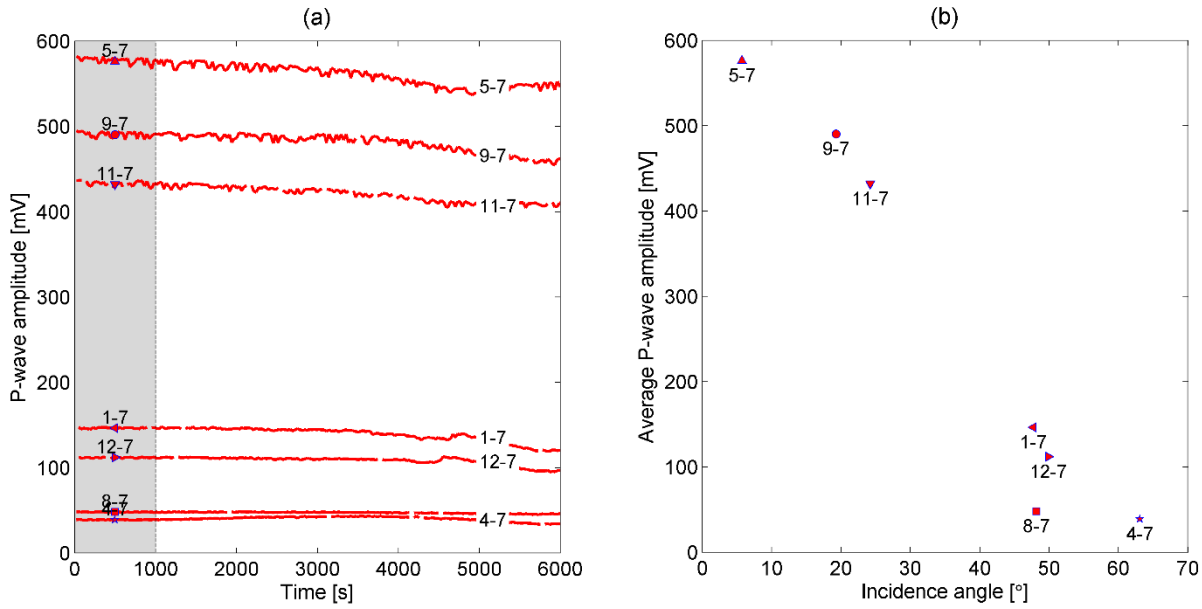

Fig. 3: Result of UT measurements (a) and resulting relative calibration (b) for the Bentheim sandstone. (a): original raw amplitudes recorded at specific ultrasonic transmitter-ultrasonic receiver pairs (the points are color coded and correspond to different ultrasonic receivers to simplify the visual inspection of the dependence of recorded amplitude on incidence angle). (b): amplitudes corrected for coupling using UTC method together with the synthetic calibration curve (thick dashed line). The estimated corrections factors are shown to the right.

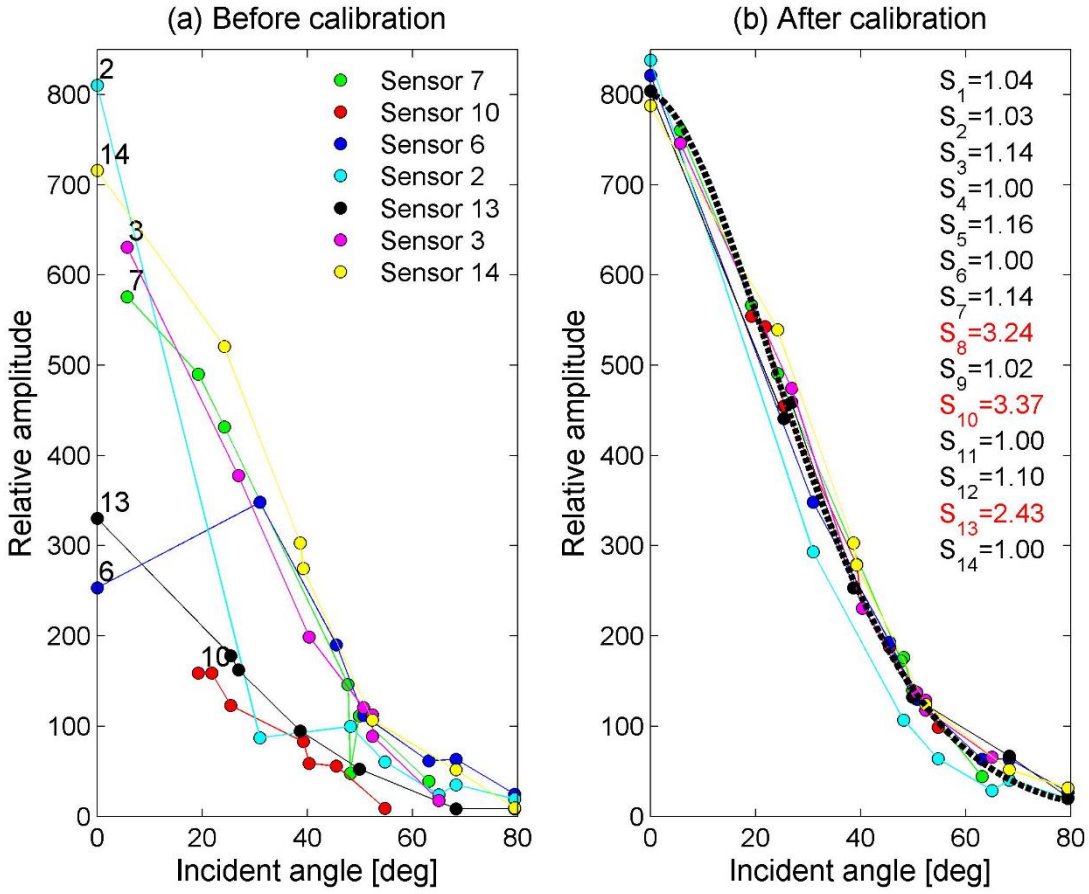

Fig. 4: Result of UT measurements (a) and resulting relative calibration (b) for the Vosges sandstone (cf. Fig. 3) for details.

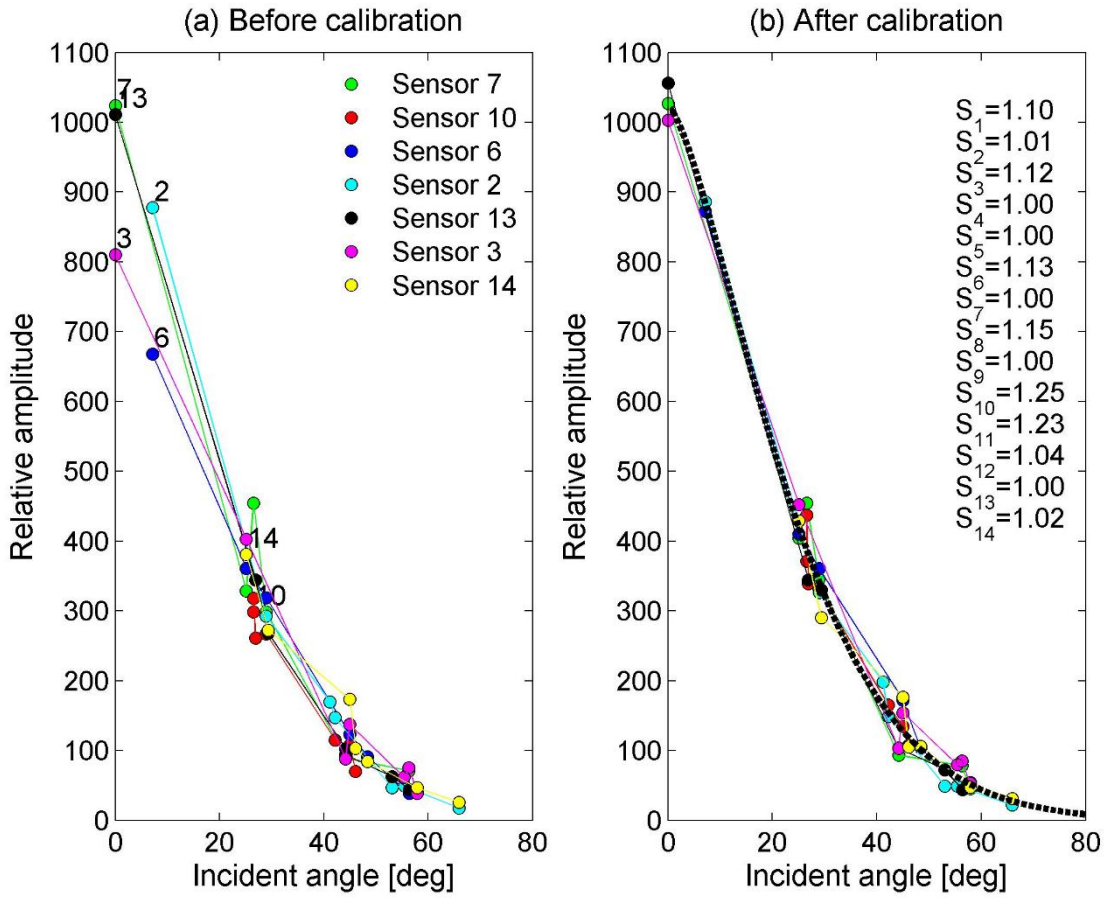

Fig. 5: Comparison of average relative RMS error distribution between the original (red) and the calibrated (blue) datasets, obtained during both triaxial experiments (left for Bentheim and right for Vosges sandstones, respectively).

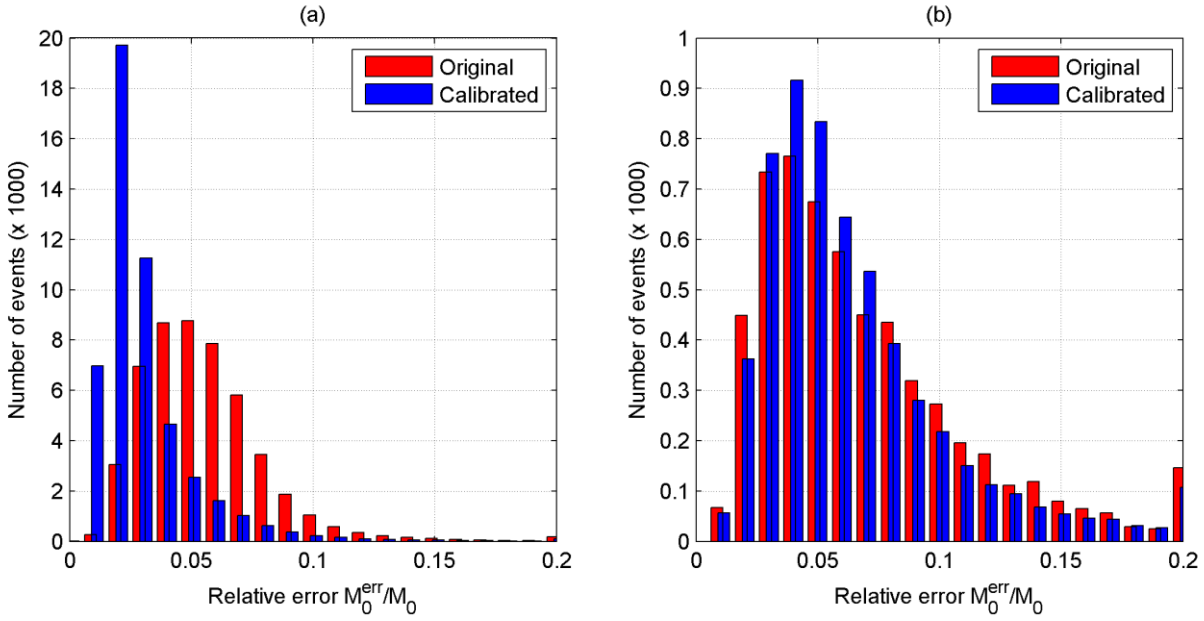

403 Fig. 6: Top view of the sample with the spatial distribution of clusters A-F (together with the number of
404 events) selected for comparison between developed calibration technique and HMT method.

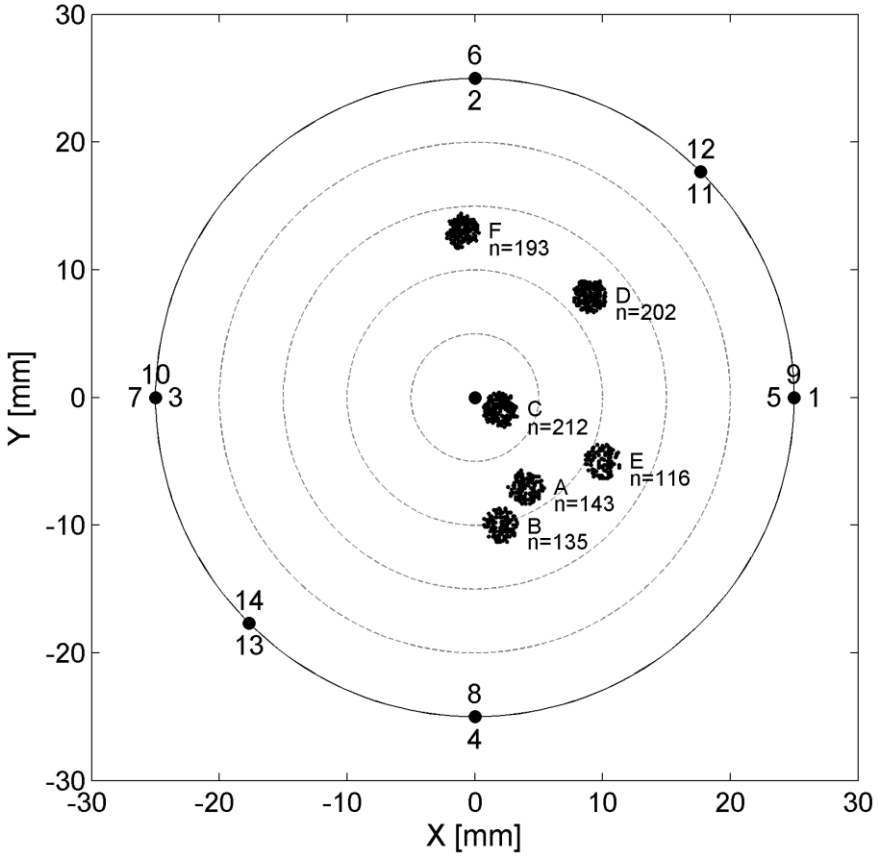

405
406

Fig. 7: Results of application of HMT algorithm to events from cluster A (cf. Fig. 6). (a): Decrease of median amplitude ratio values with progressive update of input displacement data (iteration) for each sensor. The labels correspond to sensor numbers. (b): Changes in RMS error of MTs of all events from cluster A with each iteration. (c): Amplitude correction factors of specific AE sensor (black dots) in comparison to the results of the developed calibration procedure (open squares).

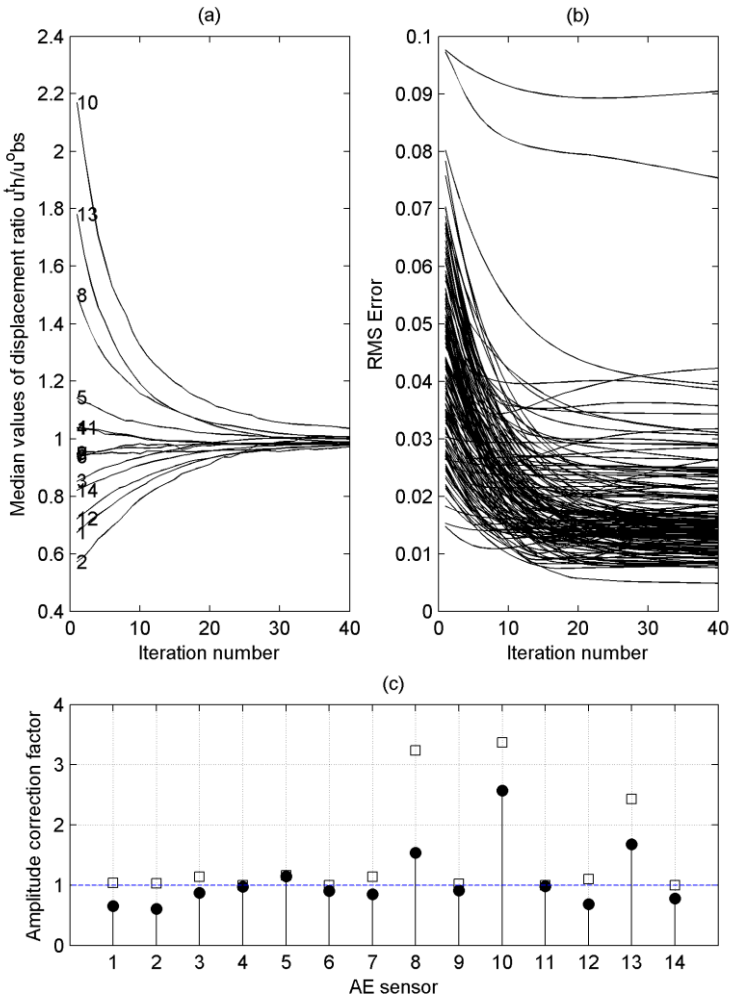

Fig. 8: Site correction factors of AE amplitudes from different clusters A-F using the HMT technique (various open symbols, cf. Fig. 6 for details). Correction factors using the UTC method presented here are shown as solid circles.

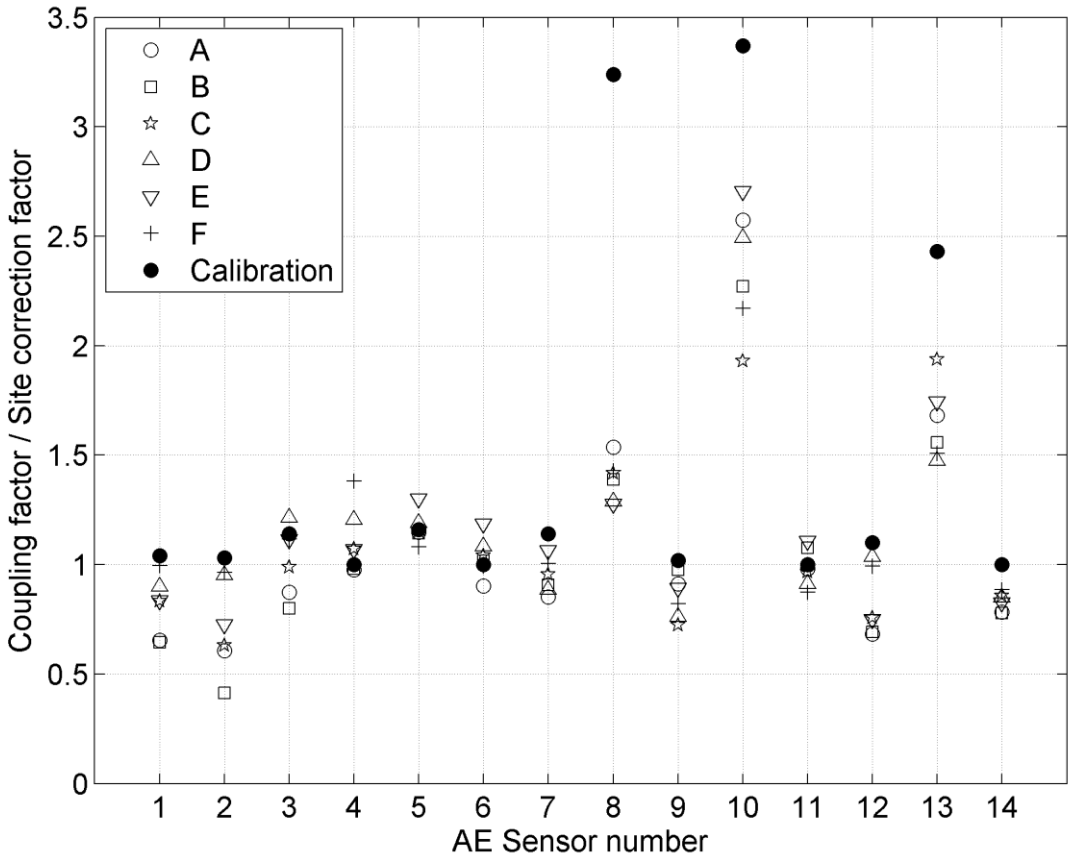

Fig. 9: Cross-section view of AE hypocenters (a, b) and corresponding source type plots (c, d) for Bentheim and Vosges sandstones. Gray and black points denote decomposed MTs before and after application of the UTC calibration method, respectively (for both datasets data up to 75th percentile of RMS error distribution of MTs are shown). AE events from Bentheim and Vosges sandstones correspond to the whole deviatoric compression part.